Determination of the singlet/triplet branching ratio in the photodissociation of ketene

Sang Kyu Kim, Young S. Choi, Charles D. Pibel, QiKe Zheng, and C. Bradley Moore

Citation: The Journal of Chemical Physics **94**, 1954 (1991); doi: 10.1063/1.459917
View online: http://dx.doi.org/10.1063/1.459917
View Table of Contents: http://scitation.aip.org/content/aip/journal/jcp/94/3?ver=pdfcov
Published by the AIP Publishing

Determination of the singlet/triplet branching ratio in the photodissociation of ketene

Sang Kyu Kim, Young S. Choi, Charles D. Pibel, Qi-Ke Zheng,[a] and C. Bradley Moore
Department of Chemistry, University of California, Berkeley and Materials and Chemical Sciences Division of the Lawrence Berkeley Laboratory, Berkeley, California 94720

(Received 23 April 1990; accepted 16 October 1990)

The rotational distributions of CO products from the dissociation of ketene at photolysis energies 10 cm^{-1} below, 56, 110, 200, 325, 425, 1107, 1435, 1720, and 2500 cm^{-1} above the singlet threshold (30 116.2 cm^{-1}), are measured in a supersonic free jet of ketene. The $CO(v''=0)$ rotational distributions at 56, 110, 200, 325, and 425 cm^{-1} are bimodal. The peaks at low J's, which are due to CO from the singlet channel, show that the product rotational distribution of CO product from ketene dissociation on the singlet surface is well described by phase space theory (PST). For $CO(v''=0)$ rotational distributions at higher excess energies (1107, 1435, 1720, and 2500 cm^{-1}), the singlet and triplet contributions are not clearly resolved, and the singlet/triplet branching ratios are estimated by assuming that PST accurately predicts the CO rotational distribution from the singlet channel and that the distribution from the triplet channel changes little from that at 10 cm^{-1} below the singlet threshold. The singlet yield shows a rapid increase in the low excess energy region (0–300 cm^{-1}), and a slower increase above. The singlet and triplet rate constants are derived from the directly measured total rate constants using the singlet yields. The triplet rate constant increases monotonically with increasing photolysis energy through the singlet threshold region. The singlet rate constant is accurately established in the threshold region and found to increase much less rapidly than predicted by phase space theory. At 2500 cm^{-1} excess energy, the $CO(v''=1)$ rotational distribution is obtained, and the ratio of $CO(v''=1)$ to $CO(v''=0)$ products for the singlet channel is measured to be 0.045 ± 0.017. This ratio is close to the variational Rice–Ramsberger–Kassel–Marcus (RRKM) calculation 0.038, and the separate statistical ensembles (SSE) prediction 0.041, but much greater than the PST prediction, 0.016.

INTRODUCTION

Unimolecular dissociations have long been of great interest because of their fundamental significance for understanding chemical bond-breaking dynamics and reaction rates, as well as for their practical importance in many chemical processes. Theoretical models for describing these reactions for ground electronic states have been subjects of controversy for many years. This is especially so for reactions without barriers to recombination of product fragments. Several models have been proposed including the Prior,[1] phase space theory (PST),[2,3] statistical adiabatic channel model (SACM),[4] SACM-PST,[5] separate statistical ensembles (SSE),[6] and the classic Rice–Ramsberger–Kassel–Marcus (RRKM) theory,[7,8] as well as recent modifications thereof.[9]

The combined application of laser and molecular beam methods makes it possible to study unimolecular reactions with the initial state of the reactant fully defined and the final quantum states of the products fully resolved. Such experiments can provide significant qualitative understanding of the dynamics of unimolecular processes as well as discriminating quantitative tests of alternative dynamical theories.

The photodissociation of ketene has been studied for decades because of the importance of methylene as a model for singlet–triplet interactions and because of the recently resolved controversy over the size of the singlet–triplet energy gap.[10] Ketene also provides a good test case for unimolecular reaction models. Ketene is excited in the UV using a transition whose oscillator strength is derived from electronic excitation to S_1. Internal conversion to S_0 and intersystem crossing to T_1 provide coupling to those two potential energy surfaces from which dissociation occurs. The T_1 triplet state correlates to $^3CH_2$ $(\tilde{X}\,^3B_1) + CO$ products 3147 ± 5 cm^{-1} below the $^1CH_2$ $(\tilde{a}\,^1A_1) + CO$ products which correlate with the ground singlet state (see Fig. 1 in Ref. 11). The ketene triplet state has a barrier to dissociation which is about 1330 cm^{-1} above the products.[12,13] The singlet state has no energy barrier above its asymptote.[14,15]

The PST model, which is based on the assumption that every product quantum state allowed by the conservation laws is equally likely to be populated, has been successful in predicting the product rotational state distribution for a system which dissociates without a barrier, but unsuccessful in predicting the vibrational state distributions and the rate constants.[11,14–16] Recently, the variational RRKM theory for unimolecular dissociation processes involving a highly flexible transition state has been developed and applied to the dissociation of ketene by Klippenstein and Marcus, and the energy and angular momentum resolved rate constants

[a] Present address: Department of Physics II, Fudan University, Shanghai, People's Republic of China.

 0021-9606/91/031954-07$03.00

for ketene dissociation on the singlet surface have been calculated.[17] In variational RRKM theory, the transition state moves in along the reaction coordinate and tightens as energy increases. Direct rate constant measurements for ketene dissociation have been made by Potter and co-workers using picosecond laser spectroscopy.[18] Theory and experiment are in good agreement. However, this comparison has been made assuming that the singlet yield increases very rapidly with increasing excess energy above the singlet threshold. In order to test the theoretical calculation more quantitatively, measurement of the singlet/triplet branching ratio as a function of the photolysis energy is necessary.

There has been an indirect measurement of the singlet/triplet branching ratio through the photofragment excitation (PHOFEX) studies in the singlet threshold region.[14,15] In the PHOFEX spectrum, the yield of one particular product quantum state is measured as the photolysis energy is scanned. All of the PHOFEX spectra probing $^1CH_2$ quantum states show a rise from threshold as the probed channels open, and then a decline at high photolysis energies as many additional singlet methylene states become energetically accessible and can compete with the specific rotational state being probed. PHOFEX spectra are reproduced very well by phase space theory (PST) for the singlet state by using the triplet rate constant as a parameter in the fitting. The triplet rate was assumed to be constant over the scan range of one PHOFEX curve and the singlet/triplet branching ratio obtained as a function of the photolysis energy in the singlet threshold region.[14,15,19] However, the uncertainties of these indirectly measured branching ratios are quite large, the assumptions open to question and the data restricted to low excess energy above the singlet threshold. In this work, the singlet/triplet branching ratio is measured from CO rotational distributions at several photolysis energies above the singlet threshold.

On the singlet surface, which has no energy barrier, the product state distribution is expected to be in some sense "statistical," since there are no strong forces favoring any particular motions of the products. On the other hand, for the triplet surface, which has an energy barrier, the position of the transition state is well defined at the top of the barrier. The product state distribution is expected to be determined primarily by the repulsive forces between the fragments as they separate from the transition state. There is experimental evidence for both cases. The CO rotational distribution from room temperature ketene photolyzed at 308 nm, where dissociation occurs mostly to singlet product, agrees well with phase space theory.[20] The CO rotational distributions from rotationally cooled ketene at photolysis energies below the singlet threshold have also been measured, they show Gaussian-shaped distributions, and have been explained using a simple impulsive model.[13] The CO rotational distribution at photolysis energies where both channels are open should be the sum of the rotational distribution from the singlet and triplet channels. When these distributions are sufficiently different, the singlet/triplet branching ratio can be determined. When combined with the rate measured for the sum of the singlet and triplet channels, the absolute rates for each channel may be determined.

EXPERIMENT

Ketene is prepared by passing acetic anhydride through a red-hot quartz tube, is trapped at 77 K and distilled twice from 196 to 77 K. Prior to use, the ketene is transferred to a bubbler maintained at 179 K, n-hexane (A.C.S. Reagent Grade) slush, where its vapor pressure is 50 Torr. Two atmospheres of He carrier gas are flowed into the pulsed nozzle after bubbling through the ketene sample. The ketene is cooled in a supersonic free jet and the rotational temperature of ketene in the jet is estimated to be 4.0 ± 0.5 K.[12]

The output of a Lamda-Physik FL2002 dye laser (0.2 cm^{-1} bandwidth) pumped by a Quanta Ray DCR-1A Nd:YAG laser is frequency doubled with a KDP crystal to produce the photolysis pulses. Mixtures of DCM and LDS 698, DCM, and Sulforhodamin 6G dyes in methanol are used to produce the resultant UV pulses from 306 to 332 nm with 5–8 mJ/pulse. The wavelength of the photolysis laser is calibrated in the red to ± 0.6 cm^{-1} by sharp Ne transitions using a Tl/Ne optogalvanic lamp (Hamamatsu).

Another dye laser (Spectra Physics PDL-3) pumped by a second Nd:YAG laser (Spectra Physics DCR-4) is used to generate the pulses around 435 nm (40 mJ/7 ns pulse) using Coumarin 440 in methanol. The beam is focused by a 7.5 cm f.l. quartz lens into a 10 cm long tripling cell filled with Xe at 20–40 Torr. The conversion efficiency of the frequency tripling process is about 10^{-6}. The output CaF_2 collimating lens (8 cm f.l.) is about 5 cm from the center of the molecular beam.

The vertically polarized photolysis beam and the horizontally polarized probe beam are counterpropagating and perpendicular to the jet. The time delay between the photolysis laser beam and the probe laser beam is fixed at around 50 ns. The laser induced fluorescence (LIF) of CO product from the dissociation of ketene is detected by a VUV PMT (EMR 542G-09-19, MgF_2 window) mounted at right angles to the laser beams and the jet about 5 cm from the interaction region. A 2.2 cm diameter CaF_2 f/1 lens and a 2.5 mm thick, cultured quartz window (Acton, CQ-1D 50% transmission at 150 nm) are placed before the VUV PMT to increase the collection efficiency and filter out the scattered light. A portion of VUV, which is not absorbed by CO, is detected by using another VUV PMT (EMR 542G-08-19 LiF window) to normalize for VUV intensity fluctuations.

The amplified signals from the PMTs are sent into gated integrators (SRS 250), digitized by an A/D interface board, and stored in a Fountain XT microcomputer. This computer is also used to trigger the lasers, scan the dye laser wavelength, and normalize the signal shot to shot.

The transitions from $X\,^1\Sigma^+$ $(v''=0, J'')$ to $A\,^1\Pi$ $(v'=3, J')$ and those from $X\,^1\Sigma^+$ $(v''=1\ J'')$ to $A\,^1\Pi$ $(v'=5, J')$ are used to determine the rotational distributions of $CO(v''=0)$ and $CO(v''=1)$ product from ketene, respectively. The CO LIF spectra show a linewidth of approximately 0.5 cm^{-1}, which is the result of a convolution of the VUV linewidth (0.35 cm^{-1}) and the spread of the ketene velocity vectors for the free jet.

The relative populations of CO rotational states are calculated from the LIF intensities by using the following for-

mula given by Greene and Zare.[21]

$$I(J'',J') \propto C(J'')S(J'',J')A_0^{(0)}B(J'',J').$$

Here the J'', J' dependence of the oscillator strength S is given by the Hönl–London factors, and $A_0^{(0)}$ is the monopole moment which is equal to unity for photofragmentation. $B(J'',J')$ is the excitation-detection configuration factor given by Greene and Zare for the mutually orthogonal geometry.[21] Any alignment factor from the photofragmentation is neglected in the population calculation. The populations from P, Q, and R branches for the same J'' state of CO show good agreement among themselves within $\pm$ 15%–20%, and these are randomly distributed, which means that the neglect of any alignment factor is a good approximation. Each data point is averaged for P, Q, and R branches over three scans.

RESULTS

The rotational state distribution of fragment $CO(v''=0)$ from ketene dissociation 10 cm^{-1} below the singlet threshold energy of 30 116.2 $\pm$ 0.4 cm^{-1}, is shown in Fig. 1 (a). The error bars are the standard deviation for a single scan and give an upper limit on all sources of random and systematic error. Since the ketene is cooled in a supersonic free jet (4 K), ketene dissociation may occur only on the triplet surface at this photolysis energy. The solid curve is a best fit to the sum of two Gaussian functions. In earlier work, the CO rotational distributions at photolysis energies below the singlet threshold were measured and the nearly Gaussian observed distributions matched a simple impulsive model including zero-point vibrational motion at the transition state.[13] However, the fit was not good for the CO rotational distribution at 29 412 cm^{-1}. This is high enough to excite the fourth vibrationally excited level of the C–C–O bending mode at the *ab initio* transition state, which contributes most of the width to the CO rotation.[13] At this level it is probably necessary to introduce anharmonicity in the C–C–O bend and it is thus not unreasonable to add a second Gaussian to the fit. Some contribution from $^3CH_2$ bending excited states must also be expected.

The $CO(v''=0)$ rotational distribution 56 cm^{-1} above the singlet threshold is bimodal, Figs. 1 (b) and 2. Since both the singlet and triplet channels are open at this photolysis energy, the CO rotational distribution is considered as the sum of the distributions from the singlet and triplet channels. Only low rotational quantum numbers are energetically accessible for CO product in the singlet channel at this low excess energy. Therefore, the peak at low J's in Fig. 2 is clearly assigned to CO product from ketene dissociation in the singlet channel and the broad peak at high J's corresponds to CO from dissociation in the triplet channel. The ratio of these two peak areas gives the singlet/triplet branching ratio at this photolysis energy. The singlet peak is fit to the phase space theory (PST) CO rotational distribution calculated as in Ref. 20 without any adjustable parameters. The curve which fits the experimental result at 30 106 cm^{-1} is used for the CO rotational distribution from the triplet channel. The solid curves in Figs. 1 (b) and 2 are the sum of

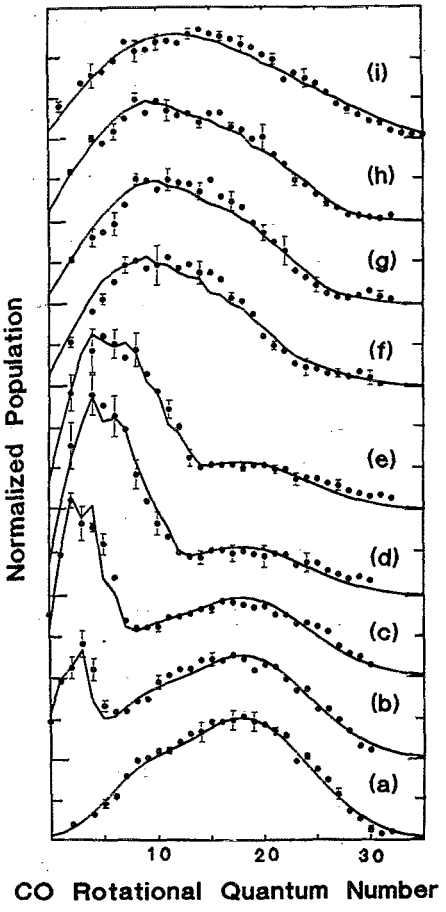

FIG. 1. The rotational distributions of $CO(v''=0)$ products from ketene dissociations at photolysis energies below and above the singlet threshold energy (30 116.2 cm^{-1}). (a): The CO rotational distribution and the fit using two Gaussians at 10 cm^{-1} below the singlet threshold. The following are the excess energies above the singlet threshold of the photolysis energies and the singlet yields corresponding to the best fits for (b)–(i). (b): 56 cm^{-1}; 0.15, (c): 110 cm^{-1}; 0.34, (d): 325 cm^{-1}; 0.60, (e): 425 cm^{-1}; 0.62, (f): 1107 cm^{-1}; 0.65, (g): 1435 cm^{-1}; 0.70, (h): 1720 cm^{-1}; 0.80, (i): 2500 cm^{-1}; 0.75.

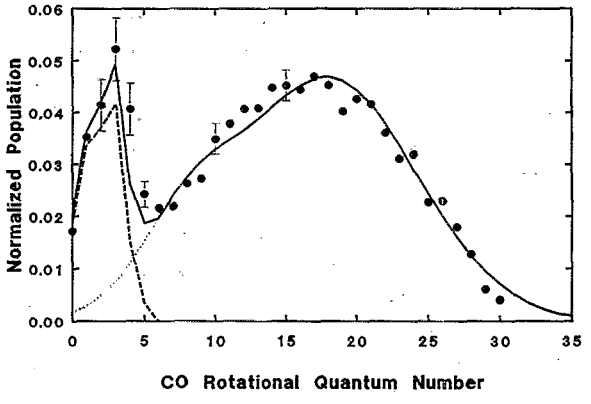

FIG. 2. $CO(v''=0)$ rotational distribution at 56 cm^{-1} above the singlet threshold is best fit with a singlet yield of 0.15. The curve (---) is the singlet contribution with a shape calculated from PST and the curve (···) is the triplet contribution.

these two distributions for a singlet yield of 0.15 and a triplet yield of 0.85. The singlet yield at this energy is thus estimated to be 0.15 ± 0.02.

The $CO(v'' = 0)$ rotational distributions at 30 226, 30 441, and 30 541 cm^{-1}, excess energies above the singlet threshold of 110, 325, and 425 cm^{-1}, respectively, are shown in Figs. 1 (c), 1(d), and 1(e). The solid curves are fits as in Fig. 2 and give singlet yields of 0.34 ± 0.02, 0.60 ± 0.06, and 0.62 ± 0.06, respectively.

Figure 1 (f) shows the $CO(v'' = 0)$ rotational distribution at 1107 cm^{-1} above the singlet threshold. At this excess energy, the high J states of CO from the singlet channel overlap the triplet channel distribution. The PST calculation for the CO rotational distribution from the singlet channel is presumed to be good even at this high excess energy and the CO rotational distribution from the triplet channel is assumed to be the same as that for 10 cm^{-1} below the singlet threshold. With these assumptions, the solid curve in Fig. 1 (f) fits the experimental data well for a singlet yield of 0.65 ± 0.07. Under the same assumptions, the singlet yields at 1435, 1720, and 2500 cm^{-1} above the singlet threshold are estimated to be 0.70 ± 0.07, 0.80 ± 0.08, and 0.70 ± 0.15, respectively [Figs. 1 (g)–1 (i)]. Especially, at 2500 cm^{-1} the overlap of the singlet and triplet distributions makes it impossible to determine an accurate triplet yield.

The branching ratios are derived from the data by assuming that PST accurately gives the CO rotational distribution from the singlet channel and that the CO rotational distribution from the triplet channel changes little with increasing photolysis energy. At low excess energies (56–425 cm^{-1}), CO rotational distributions show easily resolved bimodal distributions [Figs. 1 (b)–1 (e)]. PST calculations for CO rotational distributions from the singlet channel at these low excess energies show excellent agreement with the experimental results and CO rotational distributions from the triplet channel appear to be little changed from that at 10 cm^{-1} below the singlet threshold. At low excess energies this simple treatment works well.

But at higher excess energies, CO rotational distributions from singlet and triplet overlap, and the data do not provide enough information to simultaneously test the model assumptions and extract a singlet/triplet yield ratio. At high enough excess energy for the vibrationally excited product to be formed, the yield of the vibrationally excited product has been found to be larger than predicted by PST calculation and close to the variational RRKM prediction.[11,17,20] Klippenstein and Marcus have calculated CO rotational distributions for the singlet channel at several photolysis energies using both PST and their version of variational RRKM theory.[17] The only difference between the distributions is that the variational RRKM calculation moves population from high J's of $v'' = 0$ to the $v'' = 1$ channel. This difference is small and no attempt has been made to fit the experimental results with models other than PST for the singlet channel.

On the other hand, CO rotational distributions for the triplet channel are certainly expected to shift to higher J and to broaden as total energy increases. This has been observed,[13] but there is no reliable theory to predict the $CO(J)$ distribution from the triplet channel above the singlet threshold. The ratio of the average CO rotational energy to the total available energy [the photolysis energy minus $D(CH_2–CO)$] is 22.4% for photolysis energies below 29 412 cm^{-1}.[13] But, at 30 106 cm^{-1}, 10 cm^{-1} below the singlet threshold, the ratio decreases to 21.0%. From a straight line extrapolation to higher energies, the ratio of CO rotational energy to the total available energy for the triplet channel can be estimated to be 20%, 18%, and 16% at 425, 1435, and 2500 cm^{-1} excess energies above the singlet threshold, respectively. The corresponding Gaussian-shaped CO rotational distributions which peak at 18, 19, and 20 with ΔJ (the full widths in J) = 18, 19, and 20, respectively, can be predicted for the triplet CO rotational distributions. These Gaussian-shaped CO rotational distributions give yields which are within the error limits of the branching ratios in Table I. For data at 2500 cm^{-1}, Gaussian shaped distributions peaked at $J = 19$, 20, and 21 with $\Delta J = 19$, 20, and 21, respectively, give singlet yields of 0.75, 0.80, and 0.85. The best overall fit to the data is obtained with a singlet yield of 0.80 as shown in Fig. 3. For all photolysis energies in

TABLE I. Rate constants for dissociation of ketene as a function of energy.

Excess[a] energy	Singlet yield	log $(k_s + k_t)$	log k_t[b]			log k_s		
			Expt.	Var-RRKM	PST	Expt.	Var-RRKM	PST
56	0.15(0.02)[c]	···	8.43(0.07)	8.43	8.43	7.68(0.07)	7.68	7.68
110	0.34(0.02)	···	8.45(0.07)	8.30	8.54	8.14(0.07)	8.00	8.24
325	0.60(0.05)	···	8.50(0.05)	8.42	9.01	8.68(0.05)	8.60	9.19
450	0.62(0.05)[d]	9.04(0.03)	8.62(0.08)	···	···	8.83(0.08)	8.80	9.40
1107	0.65(0.08)	9.38(0.07)	8.92(0.09)	···	···	9.19(0.09)	9.40	10.1
1435	0.70(0.07)	9.59(0.04)	9.06(0.14)	···	···	9.43(0.15)	9.60	10.4
1720	0.80(0.08)	9.70(0.10)	9.00(0.30)	···	···	9.60(0.32)	9.75	10.5
2521	0.70(0.20)[d]	10.0(0.10)	9.33(0.37)	···	···	9.88(0.39)	10.0	10.8

[a]The excess energy in cm^{-1} above the singlet threshold of 30 116.2 cm^{-1}.
[b]The values are calculated from the var-RRKM singlet rate constants and the PST values of k_s.
[c]Errors in ( ) are estimated from the fits in Fig. 1.
[d]The singlet yields measured at 425 and 2500 cm^{-1} are used for the rate constants at 450 and 2521 cm^{-1}, respectively.

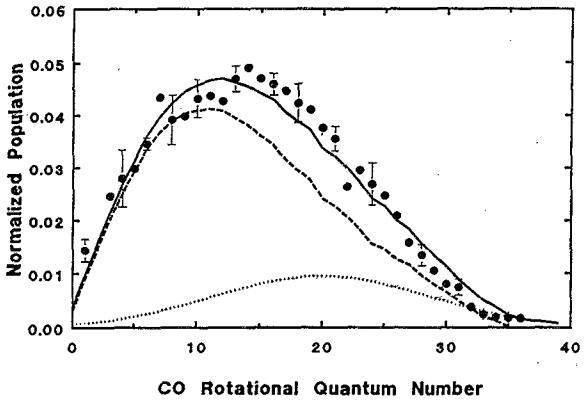

FIG. 3. CO($v''=0$) rotational distribution at 2500 cm^{-1} above the singlet threshold and a fit where the singlet yield is 0.80. A Gaussian curve (···) which peaks at 20 ($\Delta J=20$) is used for the contribution of CO from the triplet channel. The curve (---) is the PST calculated singlet contribution.

this work, vibrationally excited CO($v''=1$) from the dissociation of ketene on the triplet channel is energetically possible.[12] No significant laser induced fluorescence (LIF) signal $<0.5\%$ of $v''=0$, from CO($v''=1$) up to 1720 cm^{-1} above the singlet threshold was detected, which means that CO($v''=1$) from the triplet channel introduces a correction of less than 0.5% to the branching ratios measured from the CO($v''=0$) rotational distributions. At 2500 cm^{-1} above the singlet threshold, where the singlet yield is not much different from that at 1720 cm^{-1} (Table I), vibrationally excited CO($v''=1$) products from both channels are energetically accessible and CO($v''=1$), which is mainly from the singlet channel, is readily detected.

The rotational distribution for the vibrationally excited CO at 2500 cm^{-1} excess energy is shown in Fig. 4 with the PST calculation for the singlet channel. The overall shape of the distribution shows qualitatively good agreement with that of the PST calculation, though there is an excess population observed at relatively high J's. This extra population might be due to CO from dissociation of vibrationally hot ketene in the supersonic jet. The ratio of the CO($v''=1$) population to the CO($v''=0$) population is estimated to be 0.034 ± 0.009 after correcting for the difference in Franck–Condon factors of 0.18 for (3–0) and 0.13 for (5–1) bands[22] and summing all rotational populations of each vibrational state. The rotational dependence of Franck–Condon factors is small and neglected. The detection sensitivity of the PMT for LIF signals from the two bands is assumed to be the same for the distribution of fluorescence from $v'=3$ and $v'=5$.

DISCUSSION

The singlet yield vs excess energy above the singlet threshold shows a rapid increase in the 0–300 cm^{-1} excess energy region and a slower increase above, see Fig. 5. The total rate constant for ketene dissociation, the sum of the rate constants for singlet and triplet channels, has been directly measured as a function of energy by Potter *et al.*[18] Those measurements show that PST overestimates the singlet rate constant even for excess energies as low as 500 cm^{-1} above the singlet threshold and that a variational RRKM calculation for the singlet rate constant shows good agreement with the observed total rate constants over a wide energy range (450–5000 cm^{-1}).

The triplet rate constants at several photolysis energies below the singlet threshold have been determined by measurement of CO appearance rates.[12] An RRKM calculation gives an accurate fit to the data near threshold but predicts a much faster increase with increasing photolysis energy than the experimental results. A good fit to the experimental results was obtained by treating the triplet rate as limited by a constant intersystem crossing rate.[12] The dashed line in Fig. 6, which fits the triplet rate constants at photolysis energies below the singlet threshold, has been obtained for an intersystem crossing rate of 2.8×10^{8} s^{-1}.

From the singlet/triplet branching ratios measured in this work, it is now possible to extract the triplet and singlet rate constants from the measured total rate constants. At excess energies of 450 to 2500 cm^{-1}, the triplet and singlet

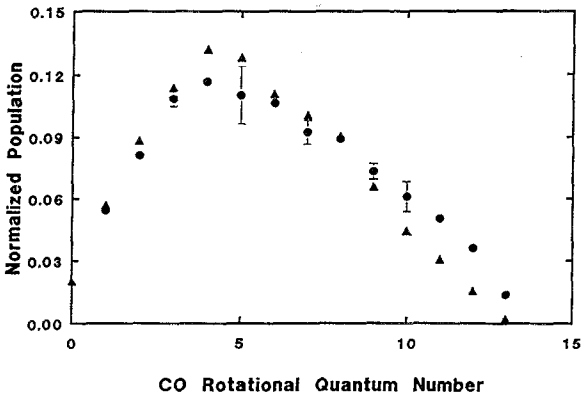

FIG. 4. CO($v''=1$) rotational distribution at 2500 cm^{-1} above the singlet threshold (filled circles), compared to the PST distribution (filled triangles). Both populations are normalized to unity for the comparison.

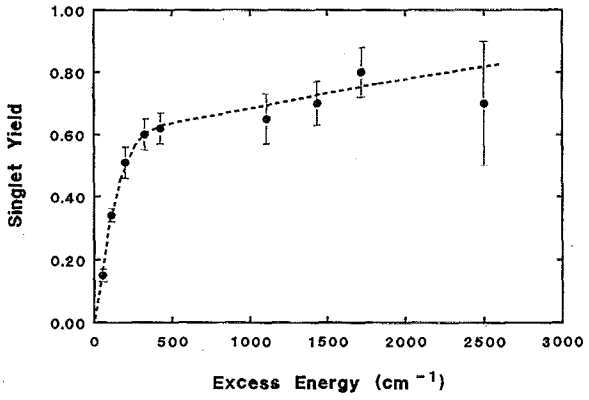

FIG. 5. The singlet yield as a function of the excess energy above the singlet threshold. The curve (---) is a smooth interpolation which is drawn just to help the eyes.

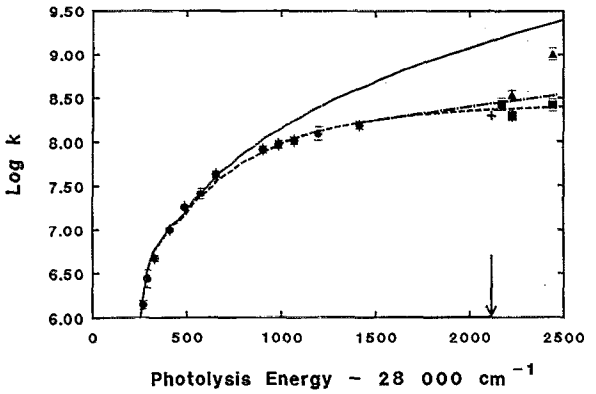

FIG. 6. The energy dependent triplet dissociation rate constant of ketene. The filled circles are the directly determined rate constants (Ref. 12). The filled triangles and squares are the triplet rate constants calculated from PST and variational RRKM singlet rate constants, respectively. At 56 cm^{-1} above the singlet threshold, both calculations give the same result. The solid curve is a RRKM calculation in Ref. 13. The curve (---) is the fit obtained for an intersystem crossing rate constant of 2.8×10^8 s^{-1}. The curve (-·-) is the smooth curve for the triplet rate constants which interpolates all experimental data as in Fig. 7. (+) point is the triplet rate constant extracted from the analysis of PHOFEX spectra of $^1CH_2$ (0_{00}) (Ref. 15). The singlet threshold energy is marked with an arrow.

rate constants are obtained from the experimentally measured total rate constants and branching ratios (Fig. 7). The singlet rate constant obtained agrees well with variational RRKM. The experimental results from Ref. 12 and this work define a smooth curve for the triplet rate as shown by the dash–dot line in Figs. 6 and 7.

This monotonic increase with photolysis energy can be explained either by treating the triplet rate as being limited by an intersystem crossing rate which increases with energy,

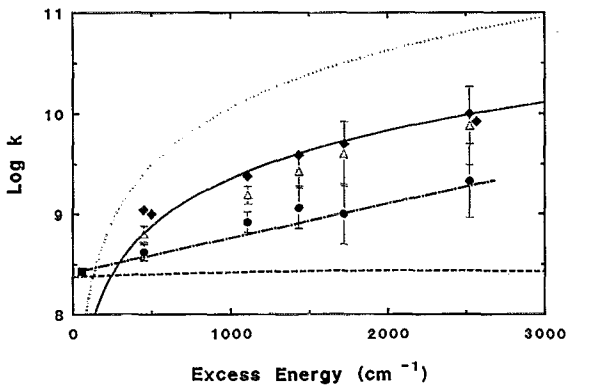

FIG. 7. Energy dependence of the dissociation rate constants. The filled diamonds are the total rate constants measured in Ref. 18. The filled circles are the triplet rate constants calculated from the measured rates and branching ratios. The filled square is the triplet rate constant calculated from the PST or variational RRKM singlet rate constant at 56 cm^{-1} where both give the same result. Open triangles are singlet rate constants from the measured total rates and branching ratios. The curve (---) is the extrapolation of the triplet rate fit obtained for an $k_{isc} = 2.8\times10^8 s^{-1}$. The curve (-·-) interpolates between the data of Fig. 6 (Ref. 12) and the data points (filled circles). The curve (···) is the PST singlet rate constant (Refs. 17 and 18)., and the solid curve represents variational RRKM calculation for the singlet rate constant (Refs. 17 and 18).

or by introducing variational RRKM theory for the triplet channel. At the singlet threshold the energy for the triplet channel is a factor of 2 greater than the barrier height. It is thus reasonable to propose, as in variational RRKM theory, that the transition state for the triplet channel may move in along the reaction coordinate with increasing excess energy. This would give a slower increase of the triplet rate constant than for standard RRKM theory.

For energies less than 400 cm^{-1} above the singlet threshold, the total rate constant measurements are not available. However, the variational RRKM and PST predictions for the singlet rate constant can be used with the branching ratios to estimate triplet rate constants. In PST, the number of open singlet channels is directly counted for the specific angular momentum, parity, and nuclear spin state of the excited ketene as a function of the excess energy above the singlet threshold. The density of reactant states is calculated by using the Whitten–Rabinovich formula,[23] multiplied by $(2J'+1)$ which is a degeneracy factor for K, and divided by four to correct for conservation of nuclear spin and parity.[15] The mean reaction time rate constant after thermal averaging for 4 K is calculated according to the method in Refs. 12 and 17. The results are shown in Table I.

At 56 cm^{-1} excess energy, variational RRKM and PST give the same singlet rate constant. If the theoretical singlet rate constant at 56 cm^{-1} is combined with the experimental branching ratio to calculate the triplet rate constant, the point falls exactly on the experimentally defined curve for the triplet, Figs. 6 and 7. Variational RRKM starts to deviate from PST near 70 cm^{-1} excess energy.[24] At 110 and 325 cm^{-1}, PST predicts a rate faster than predicted by variational RRKM by factors of 1.7 and 4.0, respectively. If variational RRKM singlet rate constants at these low excess energies (110–325 cm^{-1}) are used to calculate the triplet rate constants from the branching ratio measurements, the resultant triplet rate constants fall about 20% below the experimentally defined curve for k_t. They do show quantitatively good agreement with the fit to the low energy data obtained in Ref. 12 by assuming an intersystem crossing rate of 2.8×10^8 s^{-1}. But the triplet rate constant, which is obtained from the variational RRKM singlet rate constant and the branching ratio at 110 cm^{-1}, is about 25% smaller than for 56 cm^{-1} excess energy (Fig. 6). This suggests that the variational RRKM rates in the 100–325 cm^{-1} region are about 20% smaller than the true singlet rate constants.

If the singlet rate constants at low excess energies (110–325 cm^{-1}) are assumed to be correctly given by PST, the resultant triplet rate constants, which are calculated from the branching ratios, show a rapid increase with increasing excess energy and the triplet rate constant at 325 cm^{-1} is 2.4 times larger than that obtained from experimental data at 450 cm^{-1}. The PST rates are clearly too large. The singlet rate constant at 110 cm^{-1} can be calculated using the branching ratio measurements and the triplet curve (-·-) in Figs. 6 and 7. The logarithm is 8.14, which is between the variational RRKM calculation of 8.00 and the PST value of 8.25. At 325 cm^{-1} excess energy, $\log k_s = 8.68$ is estimated compared to the PST and variational RRKM values of 9.19 and 8.60, respectively. Therefore, the singlet rate in the low

excess energy region (56–325 cm^{-1}), seems to increase with a slope between that of variational RRKM and PST.

Recently, Klippenstein and Marcus have calculated the vibrational and rotational product state distributions for ketene dissociation on the singlet surface at several photolysis energies by using PST and their version of variational RRKM theory, which assumes adiabaticity for the conserved vibrational mode after the transition state is passed, but allows nonadiabaticity for the rotational degrees of freedom.[17] As mentioned earlier, the product rotational distributions calculated from both theories are nearly the same up to 2500 cm^{-1} excess energy above the singlet threshold. But the vibrational distributions from PST and the variational RRKM theory are different. Results for singlet methylene vibrational excitation are given in the following paper.[11] For the CO product, the ratio of $CO(v'' = 1)$ to $CO(v'' = 0)$ at 2500 cm^{-1} excess energy above the singlet threshold is calculated to be 0.038 from variational RRKM theory. The separate statistical ensembles (SSE) model of Wittig and coworkers yields 0.041, using Eq. (4) of the following paper. PST gives 0.016.[17] The experimental result in this work is $(0.034 \pm 0.009)/\Phi_s$. The singlet yield at 2500 cm^{-1} excess energy is estimated to be 0.80 ± 0.10 from Fig. 5, and the corresponding ratio of $CO(v'' = 1)$ to $CO(v'' = 0)$ is 0.045 ± 0.017. This value is much closer to the variational RRKM and SSE models than to PST.

ACKNOWLEDGMENTS

We are grateful to C. Wittig for valuable comments on this manuscript. This research was supported by the Director, Office of Energy Research, Office of Basic Energy Sciences, Chemical Sciences Division of the U.S. Department of Energy under Contract No. DE-AC03-76SF00098. S.K.K., Y.S.C., and C.D.P. thank the University of California for Dora Garibaldi Scholarship, a Charles Atwood Kofoid Eugenics, and Regents Fellowship, respectively. Q.K.Z. is grateful to the U.C. Berkeley–Fudan University Exchange Program, which made her visit to the U.S. possible.

[1] R. D. Levine and J. L. Kinsey, in *Atom–Molecular Collision Theory—A Guide for the Experimentalist*, edited by R. B. Bernstein (Plenum, New York, 1979).
[2] P. Pechukas and J. C. Light, J. Chem. Phys. **42**, 3281 (1965).
[3] C. E. Klots, J. Phys. Chem. **75**, 1526 (1971).
[4] M. Quack and J. Troe, Ber. Bunsenges. Phys. Chem. **78**, 240 (1974); **79**, 170 (1975); **79**, 469 (1975).
[5] L. Brouwer, C. J. Cobos, J. Troe, H.-R. Dubal, and F. F. Crim, J. Chem. Phys. **86**, 6171 (1987).
[6] C. Wittig, I. Nadler, H. Reisler, J. Catanzarite, and G. Radhakrishnan, J. Chem. Phys. **83**, 5581 (1985).
[7] P. J. Robinson and K. A. Holbrook, *Unimolecular Reactions* (Wiley-Interscience, London, 1972).
[8] W. Forst, *Theory of Unimolecular Reactions* (Academic, New York, 1973).
[9] D. M. Wardlaw and R. A. Marcus, Chem. Phys. Lett. **110**, 230 (1984); J. Chem. Phys. **83**, 3462 (1985).
[10] P. R. Bunker, P. Jensen, W. P. Kraemer, and R. Beardsworth, J. Chem. Phys. **85**, 3724 (1986).
[11] W. H. Green, Jr., A. J. Mahoney, C.-K. Cheng, and C. B. Moore, J. Chem. Phys. **94**, 1961 (1991).
[12] I.-C. Chen and C. B. Moore, J. Phys. Chem. **94**, 263 (1990).
[13] I.-C. Chen and C. B. Moore, J. Phys. Chem. **94**, 269 (1990).
[14] W. H. Green, Jr., I.-C. Chen, and C. B. Moore, Ber. Bunsenges. Phys. Chem. **92**, 389 (1988).
[15] I.-C. Chen, W. H. Green, Jr., and C. B. Moore, J. Chem. Phys. **89**, 314 (1988).
[16] H. Reisler and C. Wittig, Annu. Rev. Phys. Chem. **37**, 307 (1986).
[17] S. J. Klippenstein and R. A. Marcus, J. Chem. Phys. **91**, 2280 (1989).
[18] E. D. Potter, M. Gruebele, L. R. Khundkar, and A. H. Zewail, Chem. Phys. Lett. **164**, 463 (1989).
[19] W. H. Green, Jr., Ph. D. dissertation, University of California, Berkeley, 1988.
[20] D. J. Nesbitt, H. Petek, M. F. Foltz, S. V. Filseth, D. J. Bamford, and C. B. Moore, J. Chem. Phys. **83**, 223 (1985).
[21] C. H. Greene and R. N. Zare, J. Chem. Phys. **78**, 6741 (1983).
[22] R. L. Kurucz, Smithsonian Astrophysical Observatory, Special Report 374, 1976.
[23] I. W. M. Smith, *Kinetics and Dynamics of Elementary Gas Reactions* (Butterworths, London, 1980).
[24] S. J. Klippenstein (private communication).